HiSST: 2nd International Conference on
High-Speed Vehicle Science & Technology

11–15 September 2022, Bruges, Belgium

Towards high-order discretization method for hypersonic flow.

Schrooyen P.,[1] *Toulorge T.*,[2] *Coulaud O.*,[3] *Pinna F.*,[4] *Turchi A.*,[5] *Magin T.*[6]

Abstract

Classical methods to simulate hypersonic flows rely on finite volume approaches which are highly sensitive to the computational mesh and the Riemann solver chosen. This paper studies the methods to mitigate these sensibilities using high-order discontinuous Galerkin scheme. In particular, artificial viscosity and limiting methods are reviewed and compared on several test cases. Despite the loss of accuracy of limiting methods, they have been proved to be more robust to capture strong shock if combined with mesh adaptation. Artificial viscosity method relax the constraints on the mesh but numerical experiments have shown that they are less robust to capture strong shock and might require fine tuning of user defined parameters.

Keywords: *Discontinuous Galerkin, Hypersonic flow, High-order, Shock capturing*

1. Introduction

The numerical prediction of the heat flux for hypersonic flight is crucial for the design of thermal protection system. Most Computational Fluid Dynamics (CFD) codes used to simulate hypersonic flow rely on Finite Volume (FV) discretization schemes. On one hand these have shown to provide accurate evaluation of the heat flux [5, 16] but on the other hand, FV method suffers from high sensitivity to the mesh alignment with the shock and the choice of the inviscid flux function [15]. High order schemes such as Discontinuous Galerkin (DG) method offer advantages which can mitigate those drawbacks. DG discretization is promising because it provides high order accuracy on unstructured meshes, geometric flexibility, easy local adaptation in mesh size and polynomial interpolation order (h/p adaptivity). In addition, comparing to classical finite volume discretization, the scheme is highly compact and allows for a very efficient and scalable implementation. Nonetheless, the method has not been used massively for industrial applications for its lack of maturity and robustness. In particular, the method is quite sensitive to capture under-resolved features of the problem such as shocks or strong gradients [25]. Recent efforts in the DG community have been focused on improving shock detection and shock capturing method [25] showing promising results to simulate hypersonic flows [8, 26, 7].

The treatment of shocks for high-order methods is an active research field nowadays [8]. Shock fitting and shock capturing methods are the two main strategies found in the literature to treat shocks within a high-order method [24]. Shock fitting method uses a grid conformal with the shock [24] hence the discontinuity can be captured by the DG scheme. Theoretically, the method computes with accuracy supersonic or hypersonic flow if the mesh is perfectly aligned with the shock. The later is complex to ensure in practice. Indeed, even for academic cases where the shock position can be computed analytically the numerical position can be slightly different which will result in stalling or failing convergence. For unsteady computations, this requires also to adapt the mesh continuously with the position of the

[1] *Cenaero, Rue des Frères Wright 29, 6041 Gosselies, Belgium, pierre.schrooyen@cenaero.be*
[2] *Cenaero, Rue des Frères Wright 29, 6041 Gosselies, Belgium, thomas.toulorge@cenaero.be*
[3] *Cenaero, Rue des Frères Wright 29, 6041 Gosselies, Belgium, olivier.coulaud@cenaero.be*
[4] *von Karman Institute for Fluid Dynamics, Aeronautics and Aerospace Department,Chaussée de Waterloo 72, 1640 Sint-Genesius-Rode, Belgium, pinna@vki.ac.be*
[5] *von Karman Institute for Fluid Dynamics, Aeronautics and Aerospace Department,Chaussée de Waterloo 72, 1640 Sint-Genesius-Rode, Belgium, turchi@vki.ac.be*
[6] *von Karman Institute for Fluid Dynamics, Aeronautics and Aerospace Department,Chaussée de Waterloo 72, 1640 Sint-Genesius-Rode, Belgium, magin@vki.ac.be*

shock. Although extension to treat shock-shock interactions exists, the complexity makes it not ideal and therefore the method has been progressively abandoned and replaced by the prevailing shock capturing method. The shock capturing strategy proposes to capture the shock within the cell. Several methods exist to stabilize the computation among which the most important are limiting [2, 10, 4, 7], reconstruction [13, 29], artificial viscosity [32], and filtering methods [30, 22]. These methods are also common within the FV approach. This paper focuses on limiting and artificial viscosity methods. While the first one limits the order of the interpolation in the strong gradient region of the domain to control the oscillation, the second adds viscosity to smooth the solution enabling the scheme to capture it. Both methods are implemented within the Argo solver. Argo is a high-fidelity multidimensional and multi-physics platform based on a Discontinuous Galerkin discretization [14, 6, 27].

This paper will present the current effort to extend the Argo code to treat hypersonic flow. First, the equations solved and the shock capturing approaches are detailed. The advantages and disadvantages of the methods are summarized. Then, the results section analyses different tests cases to evaluate the two strategies to capture the shock. Finally, a validation test case in a high enthalpy facility is shown for the limiting strategy.

2. Mathematical formulation

First, the physical modelling to simulate the flow is described. The second subsection details the two shock capturing approaches investigated in this work. The DG scheme implemented is detailed in [14] and is not recalled in this paper.

2.1. Governing equations

The compressible flow system of equations for mass, momentum and energy conservation can be written as

$$\frac{\partial \mathbf{U}}{\partial t} + \nabla \cdot \mathbf{F}^c = \nabla \cdot \mathbf{F}^d + \mathbf{S}. \tag{1}$$

with

$$\mathbf{F}^c = \begin{pmatrix} \rho_i \mathbf{u} \\ \rho \mathbf{u}\mathbf{u} + P\mathbf{I} \\ \rho \mathbf{u} H \end{pmatrix}, \mathbf{F}^d = \begin{pmatrix} -\rho Y_i \mathbf{V_i} \\ \mu(\nabla \mathbf{u} + \nabla \mathbf{u}^t) - \frac{2}{3}\nabla \cdot \mathbf{u}\mathbf{I} \\ \tau \cdot \mathbf{u} + \lambda \nabla T - \rho \sum_i h_i Y_i \mathbf{V}_i \end{pmatrix}, \mathbf{S} = \begin{pmatrix} \dot{\omega}_i \\ \mathbf{0} \\ 0 \end{pmatrix} \tag{2}$$

where, ρ_i is the partial density of each species, Y_i is the mass fraction, $\mathbf{V}_i$ the diffusion velocity, $\mathbf{u}$ the velocity vector, P is the pressure, H the total enthalpy of the mixture and $\dot{\omega}_i$ the chemistry production term. The transport properties μ stands for the viscosity and λ for the thermal conductivity. The viscous stress tensor τ is expressed in the F^d of the momentum equation. The perfect gas law is used to close the system of equations. The Argo solver assumes thermodynamic and transport properties variable with the mixture composition and temperature but those can be set frozen during the computation. The Argo solver is linked with the Mutation++ library [28] which provides the properties and reaction terms depending on mechanism selected. For the species diffusion term, a Fick law with a Ramshaw projection is used [27]. Note that the diffusive part and source term for the mass conservation equation disappears for single species.

2.2. Shock capturing methods

Two strategies are tested within this work, limiting the polynomial order to capture the shock and adding artificial viscosity in shock region. Both are detailed hereafter.

2.2.1. Limiting

In DG discretization, the spurious oscillations in the vicinity of the shock are directly caused by the high-order interpolation used. Limiting methods lower the order of convergence near discontinuities to eliminate the spurious oscillations. Limiters are very popular in the context of standard finite volume methods because of their ease of implementation, and several extensions for high-order numerical schemes have been proposed [2, 10, 4]. The discretization of the convective terms in a DG scheme is a high order extension of a classical upwind Finite Volume Method (FVM) [14]. It can be proven that if the numerical flux is an E-flux, the Godunov scheme is positive which ensure energy stability and prevents

the local solution extrema to be increased [19]. Therefore, DGM inherits these properties from the finite volume method [27, 14]. Using a zero-order polynomial interpolation in the whole domain would therefore be equivalent as solving the problem with FVM at first order for the convective part. The naive and simplest approach to simulate hypersonic problem is therefore to degrade the interpolation order of the DG code to mimic a low order finite volume method. In order to keep the high order accuracy in smooth region, this limiting should be restricted to troubled cells.However, the order of convergence near the discontinuity is then reduced to one and the method is overdissipative [33]. More complex limiters exist but these are complex to generalize for any type of element and convergence order [1, 9, 17, 3, 12]. Compatible low order discretization using the same number of degrees of freedom can also be used in troubled cell to ensure robustness with respect to the mesh as proposed in Rueda et al.[26].

Within this work, the simplified limiting approach reduces to identify troubled cells and limit the scheme to $p = 0$ to ensure robust discretization. The Argo code features h-p adaptation which enable to degrade easily the polynomial order in the shock region. As a first step, the low interpolation order region is defined a priori. Limiting the DG-scheme in the shock region to a first order scheme (zero polynomial order), attention must be paid to the discretization of the diffusive part. The symmetric interior penalty method is not consistent at $p = 0$ since only the penalty term remains. The Bassi-Rebay 2 (BR2) method has been implemented for the diffusive part. For a scalar diffusion equation, the weak formulation becomes

$$\begin{aligned}
&\int_{\Omega_h} v_h \frac{\partial u_h}{\partial t} d\Omega \\
&- \int_{\Omega_h} \nabla v_h \cdot (\mathcal{A} \nabla u_h)\, d\Omega \\
&+ \int_{\Sigma_h} \left(\langle \mathcal{A}^T \nabla v_h \rangle \cdot [u_h] + \langle \mathcal{A} \nabla u_h \rangle \cdot [v_h] \right) d\sigma \\
&+ \int_{\Sigma_h} \langle \mathcal{A} r^{\sigma} \left([u_h] \right) \rangle \cdot [v_h] d\sigma = 0,
\end{aligned}$$

where $\langle \cdot \rangle$ and $[\cdot]$ are respectively the average and jump operator. Using the lift operator r^{σ}, it is possible to reconstruct the gradient at $p = 0$ using the jump at the boundary of each cell.

2.2.2. Artificial viscosity

Artificial viscosity method smears the discontinuities by adding artificial diffusion. It was proposed back in 1950 by von Neumann et al. [32]. The addition of a viscous term is very easy to implement and flexible with respect to the discretization scheme selected or the mesh type used. However, these methods usually rely on tuning parameters which are case-dependent and complex to determine. Recent publications have shown promising application of this method to simulate hypersonic flows [8, 31]. In this work Laplacian viscosity is added to each equation

$$\frac{\partial \mathbf{U}}{\partial t} + \nabla \cdot \mathbf{F}^c = \nabla \cdot \mathbf{F}^d + \mathbf{S} + \nabla \cdot \mathbf{F}^{art}, \tag{3}$$

where the artificial diffusive flux is

$$\mathbf{F}^{art} = \mu_{art} \nabla \mathbf{U}. \tag{4}$$

The artificial viscosity is added only in troubled cells and depends on mesh and polynomial interpolation used. To identify the troubled cells, the Argo solver uses the shock detector proposed by Persson and Perraire [25]

$$S = \log_{10} \frac{(u - u^{p-1}, u - u^{p-1})_{\Omega_h}}{(u, u)_{\Omega_h}}, \tag{5}$$

where $(.,.)_{\Omega_h}$ is the inner product defined on the element Ω_h. The variable u used to identified troubled cell is the pressure to avoid addition of viscosity in the boundary layer. A threshold S_0 is defined a priori to identify troubled cells. On a troubled cell, the artificial viscosity is defined as

$$\mu_{art,0} = c \frac{h}{p} \lambda_{max}, \tag{6}$$

where c is a scaling factor, h is the element size, p the polynomial order and λ_{max} the maximum wave speed. On the domain, combining the smoothed sensor and the elementwise viscosity (μ_0), the artificial viscosity becomes

$$\mu_{art} = \begin{cases} 0 & \text{if } S < (S_0 - \kappa), \\ \frac{\mu_{art,0}}{2}\left(1 + \sin\frac{\pi(S-S_0)}{2\kappa}\right) & \text{if } (S_0 - \kappa) < S < (S_0 + \kappa), \\ \mu_{art,0} & \text{if } S > (S_0 + \kappa). \end{cases} \tag{7}$$

Three user defined parameters remain, the sensor threshold (S_0), the scaling factor (c) and the smoothing distance (κ). To avoid fine tuning of these parameters, Vandenhoek [31] is proposing for hypersonic flow to use for the three parameters

$$\begin{aligned} S_0 &= -5\log(p) - 0.5, \\ c &= 0.27\frac{\bar{M}_\infty - 1}{\bar{M}_\infty}, \\ \kappa &= 0.5 \text{ if explicit scheme } 1.5 \text{ otherwise.} \end{aligned} \tag{8}$$

enabling to get free of tuning parameters. For transonic computation, the freestream mach number is bounded to 1.2 ($\bar{M}_\infty$) to ensure positive c. The Argo solver can either specify directly the three parameters or use the correlation proposed in Eq. 8. The computation of the artificial viscosity will lead to an artificial viscosity constant per element which can be troublesome for the convergence. To smooth the artificial viscosity field, two methods are available in Argo, the solution of an elliptic equation proposed in Ching et al. [8] or a simple averaging at the vertex of the cell. The first is computationally expensive but enables to ensure zero artificial diffusion at the wall.

3. Results

3.1. Richtmeyer-Meshkov instability

In order to study the effect of the artificial viscosity, this section investigates the results of simulating the Richtmeyer-Meshkov instability. The test case is defined in [7], the two dimensional domain is $[0, 40/3] \times [0, 40]$ on which a smoothed jump in pressure and density is set initially

$$\rho = d_{1,0.25}\left(y - \left(18 + 2\cos\frac{6\pi x}{L}\right)\right) + d_{3.22,0}(|y - 4| - 2), \tag{9}$$

$$p = d_{4.9,1}(|y - 4| - 2), \tag{10}$$

where $d_{a,b}(\cdot) = (a + 0.5(1 + \tanh(15(\cdot)))(b - a))$. Inviscid flow with single species mixture, constant thermodynamic and transport properties is assumed. The onset of instabilities and detailed flow features will depend on the resolution and dispersion of the scheme. Figure 1 shows the density field at different times on a cartesian grid of $64 * 192$ quadrangles with a $p = 3$ polynomial interpolation. The Fig. 1 compares the results for the parameters proposed in [31] (left) and the results for a tuned value of the artificial viscosity parameters (right). Values for c, S_0 and κ are compared in Table 1. The sensor proposed in [31] is more sensitive hence artificial viscosity is higher compared to the user defined parameters chosen. Small discrepancy can already be observed for early time but with lower artificial viscosity, progressively the small structures develop and lead to a different solution particularly noticeable for larger time in Fig. 1. Note that without artificial viscosity, the solver does not converge and stops prematurely. High-order methods without artificial viscosity show even better capture of the instabilities as shown in [7, 26]. While this can have a negligible effect to compute the hypersonic flow around blunt body in the absence of turbulent flow, the effect on gas-surface interaction when transition occurs should be considered.

Table 1. Artificial viscosity parameters for the Richmeyer-Meshkov.

	c	S_0	κ
user defined	0.1	-1.5	2
correlation [31]	0.07	-2.8	1.5

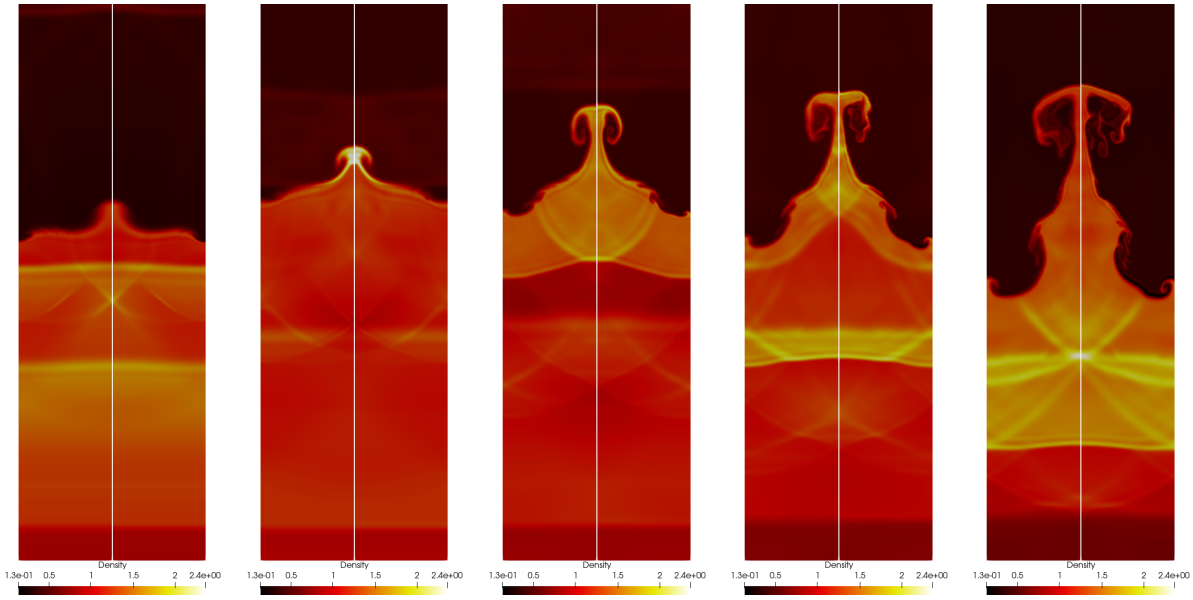

Fig 1. Richtmeyer-Meshkov instabilities for two sets of parameters for the artificial viscosity strategy. On the left, parameters proposed in [31] are used, on the right tuned values of C, S_0 and κ is used.

3.2. Flow past a cylinder at Mach 6

The hypersonic flow at Mach 6 past a cylinder is used as benchmark to compare the different strategies. The freestream conditions are given in Table 2.

Table 2. Parameters of the hypersonic test case past a cylinder.

D $[m]$	**M** $[-]$	P_0 $[bar]$	T_0 $[K]$	T_{wall} $[K]$
1.0	6	20	500	300

First, the viscous low order solution ($p = 0$) which reduces to a first order finite volume scheme is compared with a commercial code (CFD++). Both CFD++ and Argo are using the same mesh, standard CGNS format is used to convert the mesh file easily for both softwares. The mesh is refined in the shock and in the boundary layer. For Argo, the solution is constant per element and plotted as is, resulting in the step pattern that can be observed in Fig. 2. Nonetheless, a very good agreement with CFD++ can be observed. When limiting methods are used, the mesh should be sufficiently refined in the shock region to limit the degradation of the accuracy. In order to adapt the mesh (h-adaptation) to a given solution field, the strategy implemented within Argo lies in the use of metric based mesh adaptation methods for simplex [20, 21, 11]. The definition of an optimal metric space is based on the minimisation of the global interpolation error. Using the computation of the optimal metric space, the mesh is locally adapted ensuring edge length compliance with the metric and element quality. The anisotropy, minimum mesh size and complexity are user defined parameters. An example showing shock capturing for the viscous

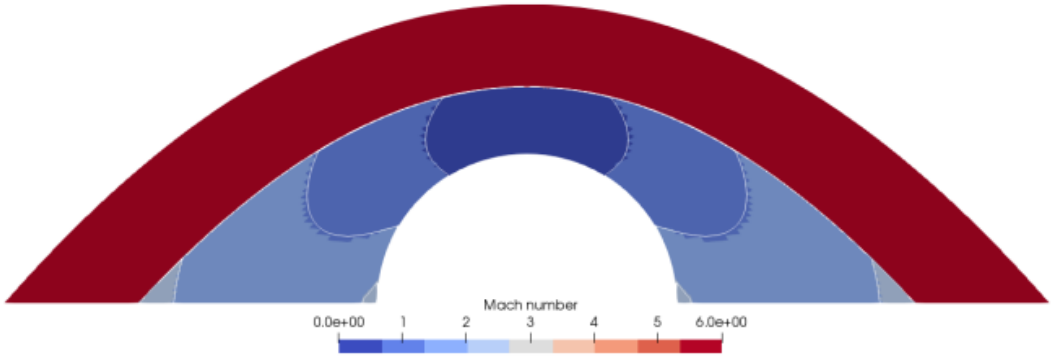

Fig 2. Hypersonic flow around a half cylinder at Mach 6. The iso-field values of the Mach number are shown for Argo and the corresponding iso-values are depicted in white for CFD++.

test case (see Table 2) is observed in Fig. 3. The meshes and convergence histories are shown for sequential adaptation. The convergence of the solver is greatly improved by using the previous solution but to compare the convergence on the different meshes, same initial solution is considered here. Note that the complexity is fixed to 1 hence the number of elements is similar in the different meshes. In order to avoid having all the elements attracted in the shock layer during the refinement, the boundary layer is frozen during the computation and quadrangles are used.

Secondly, in order to compare the shock capturing using limiting and artificial viscosity methods, the inviscid flow in same conditions is computed. We compare the solution of a variable order limiting only p in the shock region and the solution computed using artificial viscosity. The temperature field is compared in Fig. 4(a). The solution are computed on the same mesh that can be observed in Fig. 5 for which no particular attention is paid to refine in the shock region. This leads to a poor approximation limiting the interpolation to $p = 0$ in the shock as can be observed in the temperature field in the left of Fig. 4(a). For the artificial viscosity, parameters from [31] are used, the resulting artificial viscosity is shown together with the mesh in Fig. 5. As discussed previously, mesh should be refined in the shock region for limiting strategy. Figure 6 shows the comparison of the artificial viscosity with the coarse mesh (see Fig. 5) compared with a limiting strategy for which the shock region has been heavily refined. The smoothing of the shock due to the artificial viscosity method can clearly be observed along the stagnation line in Fig. 4 (b) comparing the method with limiting interpolation order on different meshes.

Analysing the robustness, the computation of a $p = 0$ solution on the entire domain (equivalent to a first order finite volume scheme) is always very robust and converges fast. When using a p adaptation reducing only the interpolation order in the shock, attention must be paid to the mesh to ensure sufficient resolution in the high-order region and mesh adaptation is required to limit area where $p = 0$. For artificial viscosity, in theory, the computation is less sensitive to the mesh but, in practice, the solution is harder to converge. Comparing to the limiting strategy, the computation per degree of freedom is more expensive in terms of CPU cost since it requires the computation of an additional diffusion term. The computational cost further increases if an elliptic equation is used to smooth the element-wise distribution of the artificial viscosity as proposed in Ching et al.[8].

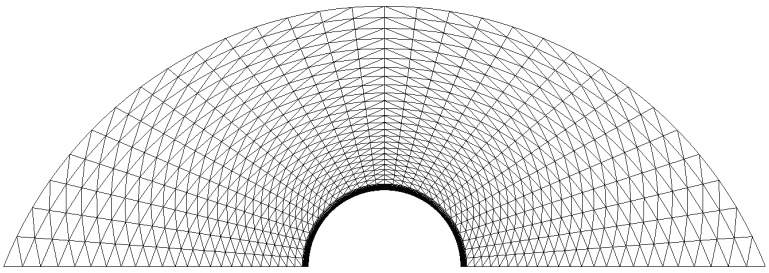

Initial mesh

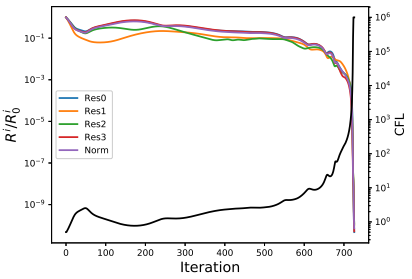

Residuals convergence

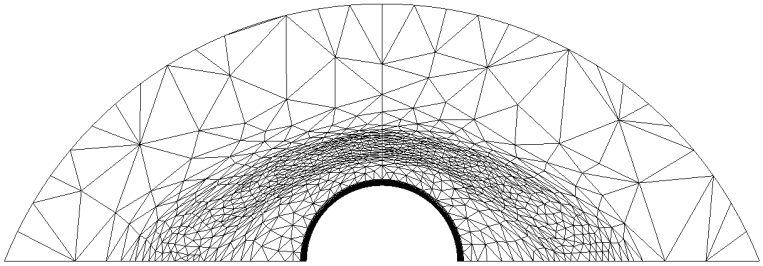

First adaptation

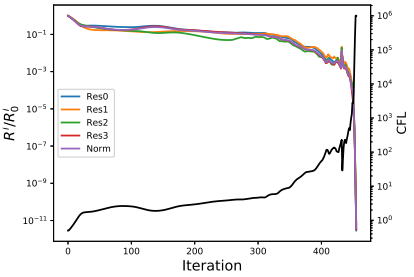

Residuals convergence

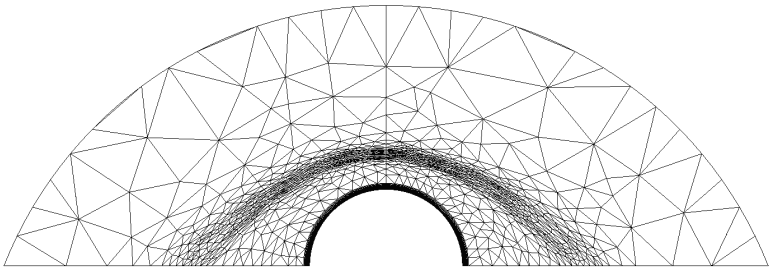

Second adaptation

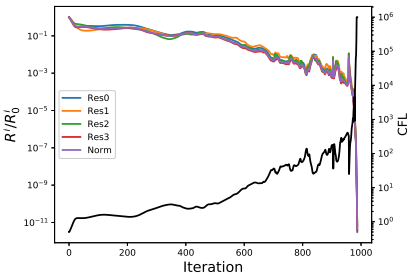

Residuals convergence

Fig 3. Sequential adaptations of the mesh for the hypersonic flow past a cylinder defined in Table 2. Boundary layer is frozen during adaptation.

3.3. Supersonic Plasmatron experiment

Previous test cases considered one species mixture with constant thermodynamic and transport properties. This test shows the capture of a shock in a high enthalpy facility. The inductively coupled Plasmatron facility operated at the von Karman institute has been recently upgraded with the manufacturing of a conical nozzle attached to the plasma torch to increase the Mach number and enable higher shear stress during the material testing [18]. The flow entering in the nozzle exits from the plasma torch. Mass flow rate and pressure measured experimentally at the torch exit are considered as inlet condition. A constant pressure is assumed at the inlet. The wall of the nozzle as well as the sample are considered as isothermal non-slip walls with a $T_{wall} = 350\ [K]$. Figure 7 shows the setup with the Mach number in the nozzle and past the sample in the chamber. The chamber pressure is imposed at the outlet.

Non-equilibrium viscous flow with 5 air species (N_2, O_2, O, N, NO) is considered with Park [23] mechanism and the problem is assumed to be 2D axi-symmetric. A polynomial order of 2 is used in the entire domain except in the shock region where the limiting procedure is applied. Within the shock region, the mesh is refined a priori.

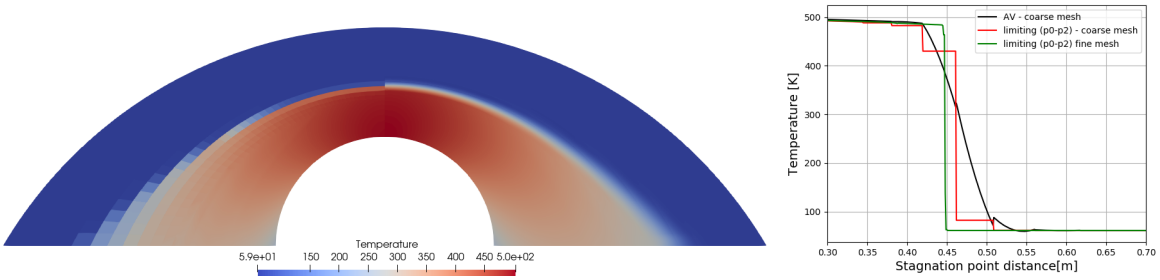

(a) Temperature field (b) Stagnation line temperature

Fig 4. Comparison of the limiting strategy and artificial viscosity method for the inviscid Mach 6 flow past a cylinder.

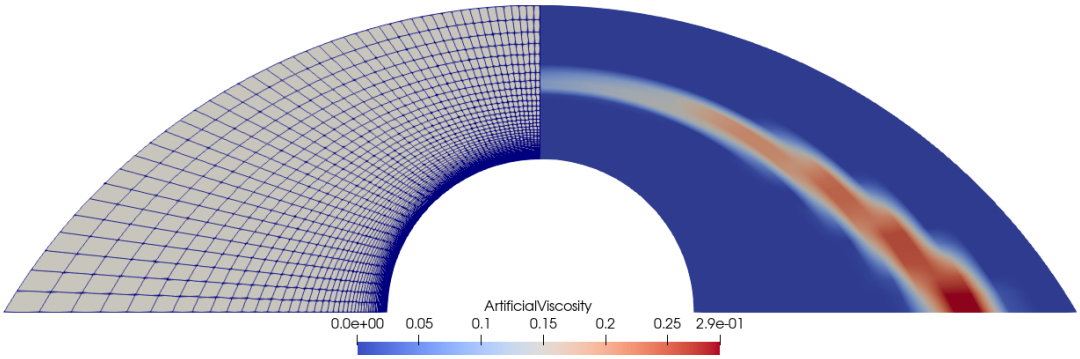

Fig 5. Mesh and artificial viscosity field to compute the flow past a cylinder at Mach 6

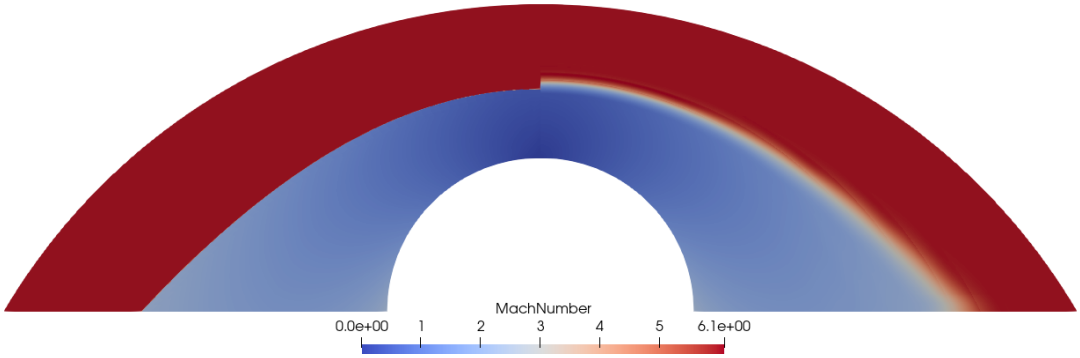

Fig 6. Comparison of the solution for flow past a cylinder at Mach 6 for a refined mesh in the shock region using limiting procedure (left) and artificial viscosity (right) computed on the coarser mesh

The shock stand-off distance is compared with the experimental picture taken during the characterization campaign in Fig. 8(a). The qualitative comparison with the shock stand off distance is good but further analysis should be performed to quantify the difference. The heat flux is also computed and is showed in Fig.8(b). To compare with experimental data, catalysis should be accounted for since the data available are measured with a copper calorimeter probe. As expected, numerical experiments have shown that the limiting strategies has the same drawback as finite volume method with respect to the sensitivity of mesh alignment with the shock.

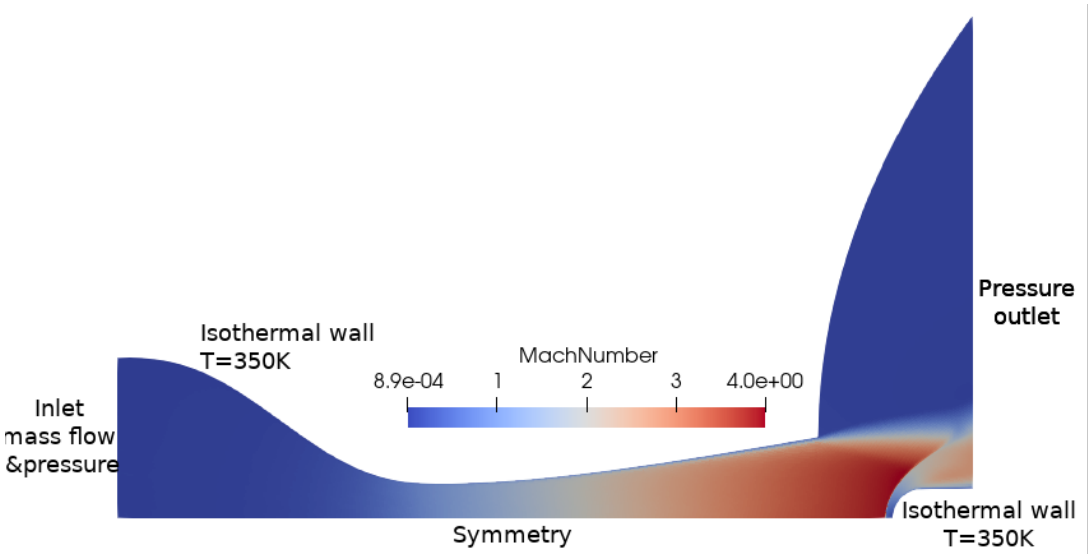

Fig 7. Numerical setup and mach number flow in the domain

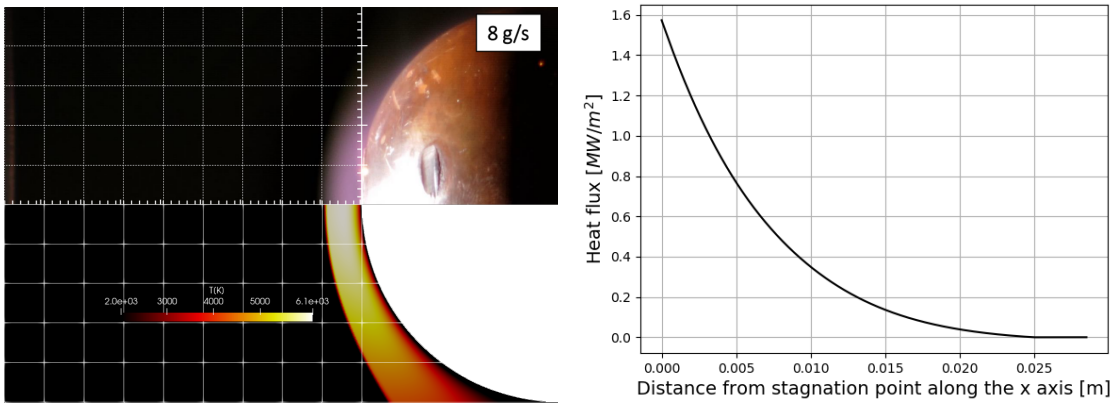

(a) Comparison with experimental data (b) heat flux

Fig 8. Comparison of shock stand-off distance with experiments (a) and heat flux along the sample (b). The experimental picture is taken by L. Sombaert [18].

4. Conclusion

Two shock capturing methods are analysed for the high-order solver Argo to simulate hypersonic flow. Artificial viscosity and low order limiting scheme are compared in academic benchmarks. Regarding the robustness, artificial viscosity method is not free of user parameters which are case dependent. Correlations proposed by [31] give a good guess for those but the solver remains difficult to converge depending on the mesh and the conditions. Limiting to a first order convergence proved to be very robust but the accuracy is greatly decreased and solver suffers from the same drawbacks as FV methods. Limiting should be activated only in troubled elements to ensure high-order accuracy in smooth regions. Hence accurate and efficient anisotropic mesh adaptation is required. These approaches are relatively easy to be implemented and more complex methods available in the literature should be tested for a proper comparison. Further comparisons should be performed in terms of robustness, accuracy and efficiency.

5. Acknowledgment

Part of this research is funded through the ESA GSTP #4000125437. The present research also benefited from computational resources made available on the Tier-1 supercomputer of the Fédération Wallonie-Bruxelles, infrastructure funded by the Walloon Region under the grant agreement #1117545. The authors would like to thank Marc Cruellas who contributed through his master thesis to evaluate the method and K. Hillewaert for several fruitful discussions on the implementation and discretization schemes.

References

[1] A. Atkins and Pampell. Robust and accurate shock capturing method for high-order discontinuous Galerkin methods. In *20th AIAA Computational Fluid Dynamics Conference*, number AIAA 2011–3058. American Institute of Aeronautics and Astronautics, 27-30 June 2011.

[2] G. E. Barter. *Shock capturing with PDE based artificial viscosity for an adaptive higher order discontinuous Galerkin methods*. PhD thesis, Massachusetts Institute of Technology, 2008.

[3] W. Boscheri, M. Semplice, and M. Dumbser. Central weno subcell finite volume limiters for ADER discontinuous Galerkin schemes on fixed and moving unstructured meshes. *Communications in computational Physics*, 25, 2019.

[4] A. Burbeau, P. Sagaut, and Bruneau C-H. A problem-independent limiter for high-order Runge–Kutta discontinuous Galerkin methods. *Journal of Computational Physics*, 169(1):111–150, 2001.

[5] G.V. Candler and I. Nompelis. Multi-Scale Turbulence Model in Simulation of Supersonic Crossflow Part 2: Inclined Injection. In *Hypersonic entry and cruise vehicles, von Karman Institute Lecture series*, Sint-Genesius-Rhode, BE, 2009. von Karman Institute for Fluid Dynamics.

[6] C. Carton de Wiart. *Towards a discontinuous Galerkin solver for scale-resolving simulations of moderate Reynolds number flows, and application to industrial cases*. PhD thesis, Université catholique de Louvain, 2014.

[7] J. Chan, H. Ranocha, A. Rueda-Ramirez, G. Gassner, and T. Warbutron. On the entropy projection and the robustness of high order entropy stable discontinuous Galerkin schemes for under-resolved flows. *Frontiers in Physics*, 10, 2022.

[8] E. Ching, Y. Lv, P. Gnoffo, M. Barnhardt, and Ihme M. Shock capturing for discontinuous Galerkin methods with application to predicting heat transfer in hypersonic flows. *Journal of Computational Physics*, 376:54–75, 2019.

[9] E. Ching, Y. Lv, and Ihme M. Development of discontinuous Galerkin method for hypersonc heating prediction. In *55th AIAA Fluid Dynamics Conference and Exhibit*, number AIAA 2012–2715. American Institute of Aeronautics and Astronautics, 9-13 January 2012.

[10] B. Cockburn and C-W. Shu. TVB Runge–Kutta local projection discontinuous Galerkin finite element method for conservation laws ii: General framework. *Mathematics of computation*, 52(186):411–435, 1989.

[11] O. Coulaud and A. Loseille. Very high order anisotropic metric-based mesh adaptation in 3d. *Procedia Engineering*, 163:353–364, 2016.

[12] M. Dumbser, O. Zanotti, R. Loubere, and S. Diot. A posteriori subcell limiting of the discontinuous Galerkin finite element method for hyperbolic conservation laws. *Journal of Computational Physics*, 278, 2014.

[13] A. Harten, B. Engquist, Osher S., and Chakravarthy S. R. Uniformly high order accurate essentially non-oscillatory schemes, iii. *Journal of Computational Physics*, 71(2):231–303, 1987.

[14] K. Hillewaert. *Development of the discontinuous Galerkin method for large scale/high resolution CFD and acoustics in industrial geometries*. PhD thesis, Université catholique de Louvain, 2013.

[15] K. Kitamura. A further survey of shock capturing methods on hypersonic heating issues. In *21st AIAA Computational Fluid Dynamics Conference*, number AIAA 2013-2698, San Diego, CA, 24-27 June 2013. American Institute of Aeronautics and Astronautics.

[16] D. Knight, J. Longo, D. Drikakis, D. Gaitonde, A. Lani, I. Nompelis, B. Reimann, and L. Walpot. Assessment of cfd capability for prediction of hypersonic shock interactions. *Progress in Aerospace Sciences*, 48:8–26, 2012.

[17] L. Krivodonova. Limiters for high-order discontinuous Galerkin methods. *Journal of Computational Physics*, 226(1):879–896, 2007.

[18] Sombaert L., Viladegut A., S. Mignano, O. Chazot, L. Desset, L. Walpot, and B. Helber. Commisisioning and characterization of semi-elliptical and conical supersonic nozzles for space debris demise testing in the VKI Plasmatron. In *2nd International Conference on Flight Vehicles, aerothermodynamics and re-entry missions and engineering (FAR)*, Heilbronn, Germany, 2022.

[19] R.J. Leveque. Numerical methods for conservation laws. Lectures in mathematics, ETH Zurich, 1992.

[20] A. Loseille and F. Alauzet. Continuous mesh framework part I: well-posed continuous interpolation error. *SIAM J. Numer. Anal.*, 49:38–60, 2011.

[21] A. Loseille and F. Alauzet. Continuous mesh framework part II: validations and applications interpolation error. *SIAM J. Numer. Anal.*, 49:61–86, 2011.

[22] A. Meister, S. Ortleb, T. Sonar, and M. Wirz. An extended discontinuous Galerkin and spectral difference method with modal filtering. *Journal of Applied Mathematics and Mechanics*, 93(6):459–464, 2012.

[23] C. Park, R.L. Jaffe, and H. Partridge. Chemical-Kinetic Parameters of Hyperbolic Earth Entry. *Journal of thermophysics and heat transfer*, 15:76–90, 2001.

[24] R. Pepe, A. Bonfiglioli, A. D'Angola, G. Colonna, and R. Paciorri. An unstructured shock-fitting solver for hypersonic plasma flows in chemical non-equilibrium. *Computer Physics Communications*, 196:179–193, 2015.

[25] P.O. Persson and J. Peraire. Sub-Cell shock capturing for discontinuous Galerkin Methods. In *44th AIAA Aeropsace Sciences Meeting and Exhibit*, number AIAA 2006-112, Reno, NV, 9-12 January 2006. American Institute of Aeronautics and Astronautics.

[26] A. M. Rueda-Ramírez, W. Pazner, and G. J. Gassner. Subcell limiting strategies for discontinuous Galerkin spectral element methods. *Frontiers in Physics*, 10, 2022.

[27] P. Schrooyen. *Numerical Simulation of Aerothermal Flows through Ablative Thermal Protection Systems*. PhD thesis, Université catholique de Louvain, 2015.

[28] J.B. Scoggins, V. Leroy, G. Bellas-Chatzigeorgis, B. Dias, and T.E. Magin. Mutation++: MUlticomponent Thermodynamic And Transport properties for IONized gases in C++. *SoftwareX*, 12:100575, 2020.

[29] C-W. Shu. Weighted essentially non-oscillatory schemes. *Journal of Computational Physics*, 115(1):200–212, 1994.

[30] E. Tadmor. Convergence of spectral methods for nonlinear conservation laws. *SIAM Journal on Numerical Analysis*, 26(1):30–44, 1989.

[31] R. Vandenhoeck. *Towards Massively Parallel and Robust High-Order Methods for Transitional Hypersonic Flow Modelling on Unstructured Grids*. PhD thesis, KU Leuven, 2022.

[32] J. Von Neumann and R.D. Richtmyer. A method for the numerical calculation of hydrodynamics shocks. *Journal of Applied Physics*, 21(3):232–237, 1950.

[33] J. Yu, C. Yan, and R. Zhao. Assessment of shock capturing schemes for discontinuous Galerkin method. *Applied Mathematics and Mechanics*, 35(11):1361–1374, 2014.